

A Qualitative Experimental Analysis of
Quasi-Two Dimensional Kolmogorov
Flow Models

by

Louis Bengtson

Submitted in Partial Fulfillment of the
Requirements for the Degree

Bachelor of Arts

Supervised by
Dr. Daniel Borrero

Department of Physics

Willamette University, College of Liberal Arts
Salem, Oregon

2019

Presentations and publications

- L. Bengtson, “A Continued Investigation of the Stability of Accretion Disks,” Willamette University, 2018.
- L. Bengtson, “Analysis of Quasi-Two Dimensional Kolmogorov Flows: The Story So Far,” Willamette University, 2018.
- L. Bengtson, “Kolmogorov Flow Analysis: Round II,” Willamette University Student Scholarship Recognition Day, 2019.
- L. Bengtson, “Analysis of Quasi-Two Dimensional Kolmogorov Flows,” Willamette University Physics Department Senior Symposium, 2019.

Acknowledgments

I think it would be a bit off-the-mark to say that this thesis has been a protracted and grueling process. It has undeniably been a lengthy undertaking, and it has certainly been tiresome at times, but in all honesty it has never weighed particularly heavily on me. This, really, is where my friends, helpers and advisors have shined their brightest. In the laboratory, Isabelle Maxwell has been a constant and patient lab partner, completing countless tasks with an admirable professionalism. Dr. Daniel Borrero has proven to be a creative and insightful advisor with whom I found myself able to communicate with the utmost ease. The other physics faculty, perhaps most notably Jed Rembold, have always been available to answer my insufferably nit-picky questions about document formatting and slideshow color schemes.

Throughout this process, I don't think I ever sincerely doubted that I was capable of completing such a thing. Really, the problem was apathy. There were certainly times when I found myself mechanically grinding through my thesis work, motivated by obligation alone, failing to stop and wonder why I ought to care at all. My motivation arose, in the end, from my fellow senior physics majors, with whom I feel a sense of camaraderie which can come only from a great deal of shared experiences. These friends, through many afternoons and evenings spent engaging in a bracing mixture of hard work, bitter complaining and hearty laughter, have shown me not only that such work is possible, but that it is worthwhile. The likes of Will Kwako, Cassie Logan, Sarah and Jill Peery, and Marcus Weaver share a zeal for science that I have aspired to emulate ever since I had the good fortune of meeting them. For this and for so very many other things, I owe them all my greatest and most sincere gratitude.

General Abstract

The behavior of fluids, ubiquitous though it may be in our daily lives, nevertheless remains quite mysterious, often completely eluding quantitative analysis due to its complexity. Only within the last century have new means of recording and analysis put the inner machinations of fluid mechanics within our sight, if not necessarily our understanding. In this thesis, we apply some of the latest methods of experimental fluid mechanics to two different permutations of the Kolmogorov flow profile, a simple model of shear flow. We hope to use the results of our experiments to examine the relationship between the flow's behavior and certain unstable solutions to the nonlinear equations that govern it. Ultimately, time is insufficient for us to be able to apply our analysis to the data we collected, but our experimental methods and the data they produced show that Kolmogorov flow is an excellent starting point for such analysis, as it can be reliably and accurately created in a laboratory setting with relatively simple materials.

Technical Abstract

Here we examine the behavior of a fluid layer driven by a time-invariant force that is periodically varying along an axis perpendicular to the axis of the forcing— the Kolmogorov flow. Utilizing electromagnetic forcing and a thin layer of electrolyte, two different permutations of Kolmogorov flow are analyzed: a “square” permutation, in which the magnetic field profile varies sinusoidally in one direction, resulting in bands of linear shear flow at low values of the Reynolds number, and a “circular” permutation, in which the magnetic field varies sinusoidally along the radial direction, resulting in ring-shaped shear flow regions. In both of these experiments, particle image velocimetry (PIV) is used to quantify flow behavior in the form of velocity vector fields. We hope to examine the relation between the quantitative behavior of the flow in state space and the presence of numerically-determined unstable equilibrium solutions to the two-dimensional Navier-Stokes equations, thereby enhancing our understanding of the quantitative nature of hydrodynamic turbulence. The “square” experiment qualitatively matches the predictions of earlier studies regarding changes in vorticity after bifurcation, and the effect of viscosity on the wavenumber of the first unstable mode of the flow, respectively. The “circle” experiment, despite having comparatively few experimental precedents, nonetheless matches qualitative expectations. Time constraints ultimately prevent numerical analysis from being performed in either experiment, but both experiments serve as validation of the utility of the quasi-two dimensional model of experimental fluid dynamics, and the groundwork is established for near-future continuation of the “circle” experiment, which will likely yield more definite quantitative results.

Table of Contents

Acknowledgments	iii
General Abstract	iv
Technical Abstract	v
List of Figures	viii
1 Introduction	1
1.1 Dynamics: A History	1
1.2 Fluid Dynamics	2
1.3 The Kolmogorov Flow	3
2 Background	5
2.1 Bifurcations	5
2.2 Navier, Stokes, and Kolmogorov	8
2.3 Running in Circles: the Kolmogorov Donut	10
2.4 Sections and Slices	11
3 General Methods	14
3.1 Forcing	14
3.2 Working Fluid	15
3.3 Image Capturing and Processing	16
3.4 JPIV	16
4 Square Configuration	18
4.1 Methods	18
4.2 Analysis	20
4.3 Discussion	22

5	Circle Configuration	25
5.1	Methods	25
5.2	Analysis	28
5.3	Discussion	29
5.4	Conclusions	29
	Bibliography	31
A	Code Used in Image Processing	33
A.1	FFmpeg	33
A.2	OpenCV	34

List of Figures

1.1	A visualization of the Mandelbrot Set, one of the most well-known fractals [Bey13].	2
1.2	An example of a flow field measured using particle image velocimetry (PIV), based on experimental data. The vector field has been color-coded to show the array of vortices that forms after several bifurcations. Regions of positive (counterclockwise) vorticity are shaded red, while regions of negative (clockwise) vorticity are shaded blue.	4
2.1	Graph of 2.1, with fixed points labeled.	6
2.2	The plume of smoke from a candle flame transitions from laminar to turbulent flow [Set09].	7
2.3	A bifurcation diagram showing a saddle-node bifurcation [Str94].	8
2.4	The basic layout of the circular Kolmogorov flow. The arrows show the directions of the two flow areas in the system's initial stable state.	11
2.5	(a): Here, $x(\tau)$ represents a trajectory in full state space, and $\hat{x}(\tau)$ represents the trajectory in the symmetry-reduced state space of the slice. The two trajectories are equivalent up to a rotational translation $g(\tau)\hat{x}(\tau)$. (b): A relative periodic orbit passes through $x(0)$, $x(\tau)$, and $x(T_p)$, returning to the point $x(0)$ after a time translation T_p . Within the slice we see the symmetry-reduced periodic orbit in which $\hat{x}(0) = \hat{x}(T_p)$. Adapted from [CBEC ⁺ 12].	13
3.1	A schematic of the first experiment's configuration, based on [TSKP ⁺ 17].	15
3.2	Copper sulfate pentahydrate crystals	16
4.1	The essential elements of the "square" experimental setup, from top to bottom: the positive and negative electrical leads, the transparent acrylic flow tank, and the aluminum base plate with inlaid neodymium magnets. Not shown are the three threaded micrometer heads that were used to level the base plate.	20

4.2	A frame from a video taken in the lab, showing the glass flow tracers suspended on the surface of the fluid. Each small white dot is actually a group of glass microspheres, which are drawn towards each other by effects related to the surface tension of the copper sulfate pentahydrate fluid. The copper electrodes in the flow tank are also visible on the left and right sides of the flow tank.	21
4.3	A sequence of three frames taken from the initial stage of a forty-second analysis of a flow bifurcation, in which the voltage between the electrodes was slowly raised from 0 to 12 V DC. (a), (b), and (c) show, in order, the first, 200th, and 400th frames out of a total of 869. The flow is initially laminar, but by the 200th frame the stripes have begun to distort, and by frame 400 the flow is beginning to resemble a lattice of vortices, rather than an array of adjacent stripes.	22
4.4	This frame from one of our flow videos shows the linear distortion which plagued our analysis.	24
5.1	Ruvim Kondratyev’s 3D-printed baseplate, with its concentric rings of Neodymium magnets. The red color of the inner rings was added to signify that they were positioned upside-down relative to the magnets in the outer rings. Copper sulfate crystals have noticeably formed at the right and bottom of the plate as a result of a minor fluid leak.	26
5.2	The circular flow configuration had only two flow bands, as opposed to the square configuration’s twelve.	27
5.3	Two different views of the circular Kolmogorov flow after its primary bifurcation. (a) shows the camera’s view—note that although the camera used in the second experiment shot in monochrome, the fluorescence of the rhodamine-resin flow tracers can still be observed. (b) shows the image resulting from PIV analysis, color coded for vorticity. The areas of strong clockwise (blue) vorticity represent boundary effects created by the walls of the tank and by the “football”, rather than areas of actual strong clockwise vorticity.	28

1 Introduction

A water faucet, when first opened, initially creates a smooth stream of water, but when the flow is increased sufficiently, the stream becomes a seething white jet of bubbles. An island creates a pattern of alternating vortices in the clouds which pass around it. These behaviors can occasionally be predicted, but for the most part they defy comprehensive description in quantitative terms. However, recent developments in the field of fluid dynamics have made new theories and methods of analysis available. This thesis, then, is motivated by the desire to apply these new ideas and methods to flows that previously have not been examined experimentally. We hope, therefore, to contribute another small step to the long process of demystifying the behavior of fluids, especially under the specific circumstances we will explore herein.

1.1 Dynamics: A History

Within the fields of physics and mathematics, the topic of dynamics is extremely broad; it denotes the study of systems that change with time. Although humans have been observing and interacting with dynamical systems since the earliest days of prehistory, the academic study of dynamics is widely acknowledged to have begun in the 17th century with Isaac Newton's invention of differential equations. Differential equations, equations that involve derivatives, are fundamental to even the most complex dynamical systems. The problem, however, is that even seemingly simple systems are sometimes governed by very complicated nonlinear differential equations, the solutions to which cannot be expressed in terms of commonly known functions—this is very much the case for the flows described here. As a result of this roadblock, the field of dynamics was somewhat limited until the advent of computers in the 1950s allowed for numerical simulations of dynamical systems. This rapid advance in understanding of dynamics led to increased interest in the concept of chaos, which had been taking a backseat to more “practical” applications of dynamics since Henri Poincaré began to consider it in the 19th

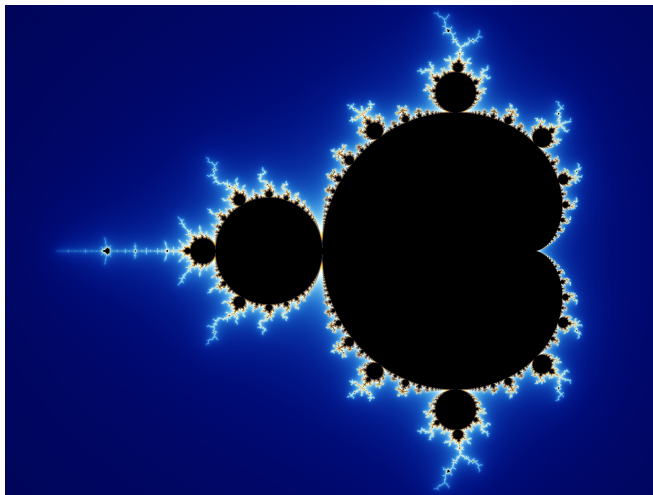


Figure 1.1: A visualization of the Mandelbrot Set, one of the most well-known fractals [Bey13].

century [Str94]. Chaos, one of the most enduringly enigmatic fields of the dynamical discipline, concerns systems that exhibit aperiodic behavior that depends sensitively on the initial conditions of the system [Str94]. The same advances in simulation technology also created great interest in the related concept of fractals, infinitely complex geometric figures which often feature repeating patterns and structures. For the first time, fractals like the Mandelbrot Set (See Fig. 1.1) could be explored visually.

1.2 Fluid Dynamics

The subject of fluid dynamics, although perhaps less popular among non-physicists than fractals and chaos theory, also benefited greatly from advances in numerical simulation technology. Fluid dynamics concerns flows in liquids, gases and plasmas, making it essential to a variety of practical applications, from engineering to art. Unlike simpler dynamical systems (a pendulum, for example), fluid flows are often extremely complex, as a fluid can take on any shape and can deform and shift in a dizzying variety of ways. Much of this complexity is due to the nonlinear nature of the equations which describe the flow— this means essentially that a change in the system’s input does not create an equivalent change in its output. Although highly advanced and efficient digital analysis and simulation software is available today, it is still often unable to represent and/or process the complexity of even a seemingly simple fluid flow. This is why, for example, water never really looks quite right when simulated in three dimensions, as one might see in a video game. In reality, the flow structure of turbulent waters is still beyond our

understanding, as researchers like Lucas [LK15] and Suri [STGS18] have pointed out. For this reason, in order to examine flows, we must often simplify them, by restricting their movement and their dimensionality.

1.3 The Kolmogorov Flow

In this thesis, we will examine the Kolmogorov flow, a type of flow which occurs when a thin layer of fluid is subjected to the following sinusoidal forcing

$$\mathbf{F} = F_0 \sin\left(\frac{2\pi x}{L}\right) \hat{\mathbf{z}}, \quad (1.1)$$

in which F_0 represents the amplitude of the driving force (the force which compels the fluid to move) and L represents the width of two opposing “stripes” of fluid [KO11]. In more qualitative terms, the Kolmogorov flow is, at low F_0 values, a pattern of “stripes” in which each stripe travels in the direction opposite to its neighbors. This neat, orderly flow can be described as *laminar*, a term denoting flows in which parallel fluid layers flow past each other without interference or mixing. The fascinating part about the Kolmogorov flow, however, is that as F_0 increases, the flow pattern begins to change. First, the stripes begin to bend and warp, no longer sliding cleanly past each other. If F_0 is sufficiently increased, they form a pattern of adjacent vortices, as shown in Fig. 1.2. If the force is increased enough, however, the flow pattern becomes highly unpredictable as the vortices break apart. At this point, we can say that the flow has transitioned from laminar to turbulent.

In this project, we aim to develop an understanding of the structures and the equations that govern the Kolmogorov flow in its various states. Although we likely cannot yet understand the Kolmogorov flow in its most turbulent and chaotic forms, we will attempt to analyze its stable solutions. The equations that govern the motion of the Kolmogorov flow have many solutions, but the stable solutions, that is, the solutions governing flow patterns that are able to withstand small perturbations, will make themselves apparent in our analysis. After all, the most commonly observed systems are those that show the most resistance to perturbation, while the more “delicate” systems are bound to change. Here, we will examine the parameters that, when sufficiently altered, will lead to instabilities in our system— qualitative changes in the system’s behavior as a result of a disturbance.

After exploring the simplest form of the Kolmogorov flow, in which the velocity profile varies sinusoidally along a linear axis, we will examine a new form, in which the flow is circular and the velocity profile varies radially. This setup, although conceptually similar, has the advantage of cylindrical symmetry, which will help us to analyze the structure of the flow. More specifically, we will be

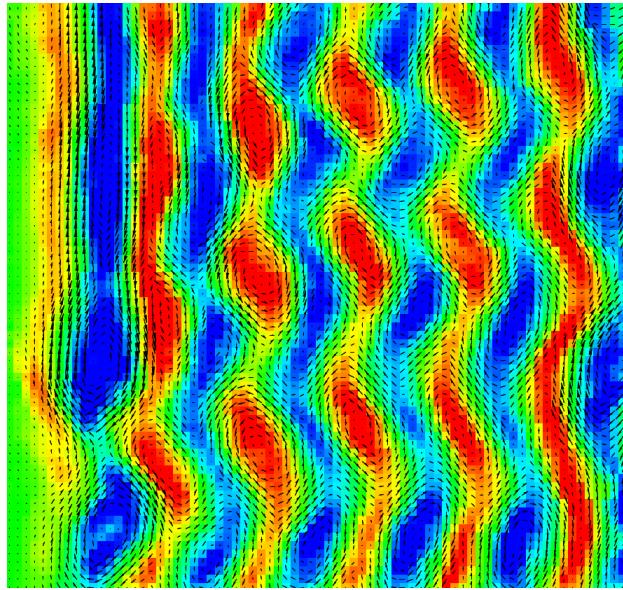


Figure 1.2: An example of a flow field measured using particle image velocimetry (PIV), based on experimental data. The vector field has been color-coded to show the array of vortices that forms after several bifurcations. Regions of positive (counterclockwise) vorticity are shaded red, while regions of negative (clockwise) vorticity are shaded blue.

looking for invariant and recurrent flow structures— structures that either remain constant or appear periodically. Much of the current research in the area of fluid dynamics, such as Kawahara [KUvV12], is focused on the search for, and analysis of, such structures and solutions. Although turbulent flows, by nature of their immense complexity, are notoriously difficult to describe or predict mathematically, researchers like Cvitanović [Cvi13] and Lucas and Kerswell [LK15], among others, have made significant headway in recent years. This project, then, will hopefully represent another small step towards a more complete understanding of the flows that have only recently become accessible to analysis.

The remainder of this thesis is organized as follows: Chapter 2 will explore the theoretical background that underlies bifurcation theory and will introduce the method of sections and slices; Chapter 3 will describe the elements of the experimental setup and of the analysis that were common to both the square and the circular flow configurations; Chapter 4 will contain the methods and analysis unique to the square flow configuration, and a discussion thereof; Chapter 5 will be similar to Chapter 4, but will cover the circular flow configuration. Finally, Appendices A and B, respectively, will detail the operation of the PIV software used in the experiments as well as the other code used for image processing.

2 Background

Fascinating as it is from a qualitative perspective, we can learn very little about Kolmogorov flow by merely observing it. In order to better understand the flow's behavior we must explore the fundamental concepts of fluid dynamics, and discuss how these concepts can be applied, or at the very least related to the modern methods of flow analysis that will be implemented in later chapters.

Much of the enduring fascination with the Kolmogorov flow within the field of fluid dynamics comes from its utility as a simple model of shear flow. In recent decades, increased attention has been given to this model, and new theoretical frameworks have been developed to allow more informative analysis of both simulated and experimental Kolmogorov flows. In this chapter, we will explore the theory behind the behavior of the Kolmogorov flow. We will begin with a discussion of bifurcations, the changes that occur in the system's behavior as its parameters are altered. We will then examine the Navier-Stokes equations, optimizing them for our purposes to describe the Kolmogorov flow, and finally we will define the Reynolds Number, an essential quantity for understanding flow behavior. Although this thesis presents primarily an experimental analysis, and not a theoretical simulation, we must assume that the same theories that can create a flawless simulation can also underlie the inevitably imperfect flows we create in the laboratory, and so they ought to serve as the basis of our discussion.

2.1 Bifurcations

As we discussed earlier, dynamical systems are governed by differential equations. Here we will focus for a moment on the topic of equilibrium solutions to differential equations. Our discussion will borrow from Strogatz [Str94], whose book *Nonlinear Dynamics and Chaos* is an excellent primer on the topic. Consider, for example, the following differential equation:

$$\dot{x} = x^2 - 1 \tag{2.1}$$

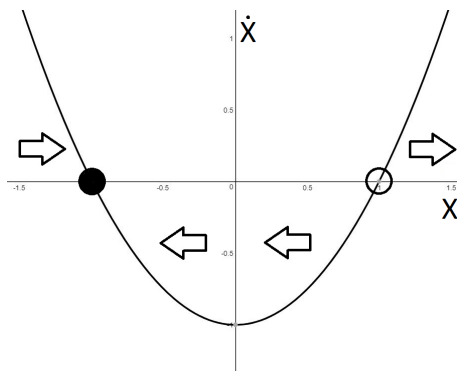


Figure 2.1: Graph of 2.1, with fixed points labeled.

Graphing \dot{x} vs. x , as shown in Fig. 2.1, one can easily see that the function is equal to zero when $x = \pm 1$. Because x does not change when \dot{x} is zero, we call these the equilibrium solutions to the differential equation. To better visualize the problem, let us imagine that the function represents the motion of a rolling ball. Inasmuch as \dot{x} represents the change in x over time, we can say that when the function is above zero, the ball’s velocity is positive, and the ball is moving to the right, and when the function is below zero, the opposite is true, as shown by the arrows on the graph.

Judging by the arrows, we can easily say that $x = -1$ is a stable equilibrium point, or a stable “fixed point”; if the ball is at this point, a small push to the left will only cause it to roll back to the right, and a small push to the right will lead it to roll back to the left, eventually settling down at its original position. By contrast, $x = 1$ is unstable; if the ball is at this position, almost any amount of disturbance will cause it to roll away (to infinity, if it is pushed to the right). However, if the ball is located at $x = -1$, and it is given a sufficiently hard push to propel it past $x = 1$, it will roll away as well. So, we cannot say that $x = -1$ is completely stable. Instead, we must say that it is “locally stable” [Str94]. In this type of system, all solutions must either settle down to equilibrium or run off to infinity.

These behaviors, and the locations at which they occur, depend on the parameters of the system, and changes in the parameters will result in changes in the system’s behavior. For instance, if Eqn. 2.1 were changed to be $\dot{x} = x^2 - 2$, the “fixed points” would have new locations—namely, $x = \pm\sqrt{2}$.

In order to more fully understand the workings of the Kolmogorov flow and its dramatic transitions, we must become acquainted with the idea of bifurcations. Generally speaking, a bifurcation is a qualitative change in the behavior of a system. Bifurcations are the source of all the complexity in dynamical systems, and the reason why they are generally unpredictable. In many cases, one bifurcation leads to another, and another, resulting in rapid and dramatic changes in the



Figure 2.2: The plume of smoke from a candle flame transitions from laminar to turbulent flow [Set09].

flow’s qualitative behavior. For example, Fig. 2.2 shows a simple flow undergoing a series of bifurcations leading rapidly to chaotic turbulence.

Bifurcations, no matter how random and mysterious they may seem, cannot happen unprompted. Every bifurcation is the result of a change in some aspect of the system, which we can call a bifurcation parameter. In the previous example, the bifurcation parameter was the constant integer added to x^2 . Let us then rewrite the equation as follows:

$$\dot{x} = x^2 + r. \quad (2.2)$$

Here, r will generally represent our bifurcation parameter. It stands to reason that if $r > 0$, the system will have no fixed points. The entire curve will be positive, so any “ball” placed anywhere on it will roll away to the right (and judging by the curve, it would reach quite a terrific speed). If $r = 0$, the curve will have exactly one fixed point, at $x = 0$, a point which we can call *hyperbolic*, or “half stable”. At this type of fixed point, the ball-on-a-hill analogy breaks down a bit. A ball placed to the left of $x = 0$ will travel to the right, continually slowing down until it stops at $x = 0$, while a ball placed anywhere to the right of $x = 0$ will roll away to infinity. A ball placed at $x = 0$ will return to its starting position if pushed to the left, and will roll away if pushed to the right. Hence the designation, “half stable”. Finally, if $r < 0$, the system will have two fixed points, one stable and one unstable, as discussed before. Taking all this information into account, we can now graph x , here denoting the fixed points, as a function of r , as shown in Fig. 2.3. For reasons that have more to do with a three-dimensional version of this system, this is called a *saddle-node bifurcation*, and is one of the most common in simple systems.

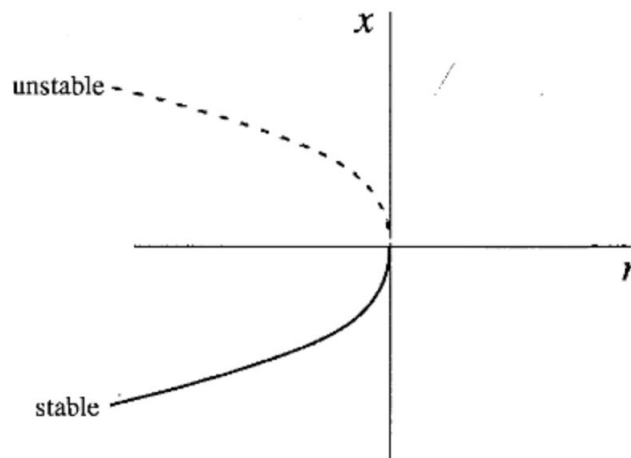


Figure 2.3: A bifurcation diagram showing a saddle-node bifurcation [Str94].

In one-dimensional dynamical systems, bifurcations are rarely very interesting, because all behaviors in the system either reach equilibrium or run off to infinity. Take, for example, a box on the end of a spring, constrained to move back and forth in one direction. If we change the mass of the box, we can quantitatively change the behavior of the system; the spring may oscillate more slowly, and may come to a stop more quickly. However, the qualitative behavior of the system will not change—the box will still move back and forth in a straight line. In a higher-dimensional system, more complex qualitative behavioral changes are possible. For instance, consider the same spring and box from earlier, but this time it is allowed to move in two dimensions, to wiggle from side to side. If the box, while moving back and forth in the \hat{x} direction, is given a sudden push in the \hat{y} direction, its behavior will change in a way that will depend largely, if not entirely, on the other parameters of the system—the mass of the box, the stiffness of the spring, the initial position and velocity of the box, etc.

2.2 Navier, Stokes, and Kolmogorov

Fluid flows, unsurprisingly, are quite a bit more complex than the previous examples. First and foremost, they have quite a few more dimensions. Fluid flow is a continuum, meaning that when we analyze it, we are not focusing on a single object's motion, as in the case of a ball on a hill or a box on a spring. Rather, we are focusing on the motion of a continuous substance. Instead of having a single velocity and a single position, a fluid flow is made up of a theoretically infinite number of fluid elements, each with its own velocity, position, and so on, which makes the dynamics of the fluid infinite-dimensional. Even when flows are simulated computationally using vector fields, many simulated points must be used,

which still leads to a very high-dimensional system. However, such flows are not unmanageable, especially when some key factors are taken into account. First of all, in this case our flow will be quasi-two dimensional, which essentially means that two of its dimensions are much greater than the third, or that its surface area is much greater than its depth. Since in this thesis we will only examine the flow that occurs on the very surface of a fluid layer, the quasi-two dimensional simplification is a natural one. This reduction in dimensions will greatly simplify both the theoretical aspects of this thesis, explored shortly, and the experimental aspects, presented in the coming chapters. Secondly (drawing from the derivation presented by Kelley and Ouellette [KO11]), we will benefit greatly from the fact that fluid flows are bound by conservation of momentum, which in this case can be written as

$$\frac{\partial \mathbf{u}}{\partial t} + (\mathbf{u} \cdot \nabla) \mathbf{u} = -\frac{1}{\rho} \nabla p + \nu \nabla^2 \mathbf{u} + \mathbf{f}. \quad (2.3)$$

Here, $\mathbf{u} = u\hat{\mathbf{x}} + v\hat{\mathbf{y}} = (u, v)$ is the two-dimensional velocity field, t is time, ρ is the mass density of the fluid, p is its pressure, ν is its kinematic viscosity, and \mathbf{f} is the applied force [KO11]. Additionally, we will assume that the fluid in our experiment is incompressible (this is a safe assumption for low speeds), meaning

$$\nabla \cdot \mathbf{u} = 0 \quad (2.4)$$

In other words, the divergence of the velocity field is zero. Equations 2.3 and 2.4 are known as the Navier-Stokes equations, and they will be critical to our understanding of the Kolmogorov flow.

In order to eliminate the pressure term from Eqn. 2.3, we can rewrite it as

$$\frac{\partial \boldsymbol{\omega}}{\partial t} + (\mathbf{u} \cdot \nabla) \boldsymbol{\omega} - (\boldsymbol{\omega} \cdot \nabla) \mathbf{u} = \nu \nabla^2 \boldsymbol{\omega} + \mathbf{F}, \quad (2.5)$$

in which $\boldsymbol{\omega} = \nabla \times \mathbf{u}$ represents the vorticity and $\mathbf{F} = \nabla \times \mathbf{f}$ represents the forcing applied to the system [KO11]. In reality, this equation is an oversimplification as it fails to account for several factors. First, our flow is, of course, not truly two-dimensional, meaning that there ought to be $\hat{\mathbf{z}}$ components in the \mathbf{u} and \mathbf{F} terms. Secondly, Eqn. 2.5 fails to account for the drag occasioned by the interaction between the fluid and the bottom of its container. These inconsistencies, however, are minor enough that we can ignore them for the time being.

The most basic solution to Eqn. 2.5 is the aforementioned group of stripes, each stripe moving opposite to its neighbors, which occurs when the forcing is low. Quantitatively, this solution is characterized by

$$\mathbf{u}_0 = \sqrt{3}U \cos\left(\frac{2\pi x}{L}\right) \hat{\mathbf{y}} \quad (2.6)$$

$$\boldsymbol{\omega}_0 = \nabla \times \mathbf{u}_0 = -\sqrt{3}U \frac{2\pi}{L} \sin\left(\frac{2\pi x}{L}\right) \hat{\mathbf{z}}, \quad (2.7)$$

in which $U = \langle \mathbf{u}_0 \cdot \mathbf{u}_0 \rangle^{1/2}$ is the root-mean-square velocity [KO11].

Although Eqns. 2.4 and 2.5 characterize the motion of our system, and Eqns. 2.6-2.7 describe its most basic state, it would still be quite convenient to define a quantity that could be used to characterize the overall stability of the system. This dimensionless quantity is the Reynolds Number Re , defined as

$$Re = \frac{UL}{\nu}, \quad (2.8)$$

although, in the interest of clarity, it can also be described as

$$Re = \frac{\text{Inertial Forces}}{\text{Viscous Forces}} \quad (2.9)$$

The Reynolds Number is especially useful in the analysis of fluid flows because it relates two important concepts: viscous damping and fluid inertia. Viscous damping is the ability of a flow to resist, or “damp”, small disturbances, and is what allows some types of flow to be considered stable. Fluid inertia, in this case, lends itself to flow instabilities. It can be thought of as the force exerted due to the momentum of a fluid.

In our experiment, Re will characterize the overall complexity of the system, and will function as our bifurcation parameter, determining when the flow will transition from laminar to turbulent, and when it will experience instabilities. At low values of Re , the system will remain in the stable state described by Eqn. 2.6, a state in which the viscous effects of the flow will damp out small disturbances. At a sufficiently high value of Re , however, the flow will bifurcate into a lattice of vortices, as shown in Fig. 1.2. One of our early goals here will be to determine the critical values of Re , i.e., the values at which the flow experiences significant instabilities.

2.3 Running in Circles: the Kolmogorov Donut

The Kolmogorov flow, worthy of study as it is, has been studied quite a bit [The92] [BBM⁺99] [STM⁺14], and although it provides a nice opportunity to get acquainted with nonlinear and fluid dynamics, it is relatively unlikely that our analysis will turn up anything new. With that in mind, we will now introduce a new concept; that of a circular Kolmogorov flow. That is, we will additionally explore a Kolmogorov flow setup in which the velocity profile varies radially, as shown in Fig. 2.4. This setup will function similarly to the previously discussed arrangement, and in the most basic sense, will have the same qualitative behavior. At low values of Re , it is expected that the opposing flows will be laminar, while at high Re values, instabilities should appear. One advantage of this approach is

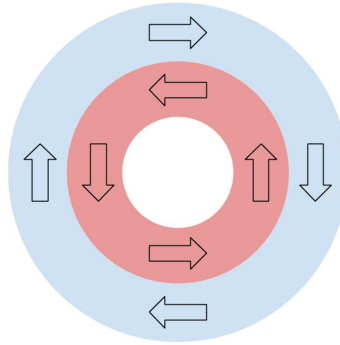


Figure 2.4: The basic layout of the circular Kolmogorov flow. The arrows show the directions of the two flow areas in the system’s initial stable state.

that it will help us to avoid some of the inconveniences imposed by the previous model; namely, some of the problems caused by walls. Of course, our second setup will still have walls on the inside and outside of the “donut”, and these walls will create the same unwanted drag effects as the walls in the previous setup. However, because of the circular shape, the bands of fluid will be able to flow continuously past each other without running directly into a wall. This is roughly analogous to the periodic boundaries employed in many flow simulations, in which flow exiting one side of the simulated area reappears on the other side, with the goal of approximating an “infinite” simulation area.

2.4 Sections and Slices

One of the most significant advantages of the “donut” setup is that it will allow some flow structures to progress around the circle without experiencing boundary interference. In the square setup, a travelling structure can only move so far before it must either make a sharp U-turn or run into a wall, either of which would certainly change its shape and behavior. By contrast, a flow structure in the circular setup can travel around the circle and return to its initial position without deviating or deforming too much. Qualitatively, this system is somewhat simple. Quantitatively, it is anything but. Our analysis, as mentioned earlier, is based on the search for recurring structures in the flow. To that end, we intend to make use of the symmetry of the flow to find flow structures known as relative periodic orbits, which we will discuss below, and then use reduction of symmetry to turn them into ordinary periodic orbits.

In order to understand these concepts, we’ll have to take a trip into high-dimensional space. First, we will define the important parameters of our flow; positions and velocities. That is, each of the infinitely many points in a flow has its own position, and its own velocity vectors in the \hat{x} and \hat{y} directions (assuming, as

we are, that the flow is two-dimensional). So, any point in the flow can be summed up by a list of numbers. The entire system, then, can be described by combining all the individual lists into another (very, very large) list of numbers. Since we cannot process an infinite-dimensional system, we will approximate the flow by using a much smaller number of points, perhaps in the thousands. Although a system with tens of thousands of dimensions might seem very hard to imagine, let alone analyze, it is entirely possible. Because the entire system at any given time can be described by a list of numbers, each of these numbers could be treated as its own dimension, and the entire system could then be imagined as a single point in a multi-dimensional state space, with the whole of state space representing the collection of all possible flow profiles.

We cannot create a graph with thousands of axes, but a graph with only three can serve as a reasonable approximation, surprisingly enough. Because the system, at a moment in time, can be depicted as a point in state space, any evolution of the system in time will result in a new list of numbers describing the system, and thus a new point in state space. Or, rather than a new point, a translation of the original point. As the system evolves in time, then, its point traces out a *trajectory*.

If a system evolved in such a way that its trajectory eventually returned to precisely its initial point, we would call this behavior a periodic orbit. In Kolmogorov flow, periodic orbits are generally hyperbolic (essentially meaning that they are attractive from certain directions, but repulsive from others), and are very difficult to observe directly in experimental scenarios, inasmuch as a system's trajectory will often draw close to a periodic orbit for only a short time before being repelled by the orbit's instability [LK15]. Not all periodic orbits, however, are created equal. Some are more unstable than others, and it stands to reason that a trajectory will spend more time in the vicinity of less-unstable periodic orbits. This means, therefore, that the behavior of a flow can, to a certain extent, be predicted by examining the periodic orbits around which it spends the most time.

Another complication, however, presents itself at this point in our discussion. That is, we must take into account that spatial structures in the flow may reoccur without returning to precisely the same point in state space. If a particular arrangement of velocity vectors, for example, were to appear in two different places in the circular flow, it would be structurally identical in both places, but entirely different in state space due to its change in position. This we can call a relative periodic orbit. Although relative periodic orbits are common in turbulent flows, and can be identified numerically without too much trouble, they present a problem for analysis, namely, their complexity. That is, a relative periodic orbit is not a simple loop in state space. Instead, it is a loop that has been extruded along a trajectory, resulting in an (often misshapen) torus composed of an infinite number of loops (see Fig. 2.5). This poses a problem, of course; such

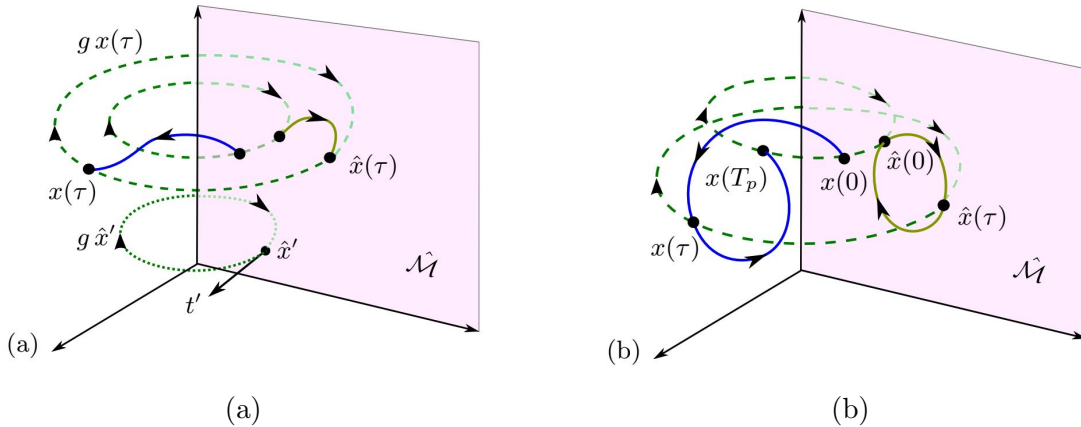


Figure 2.5: (a): Here, $x(\tau)$ represents a trajectory in full state space, and $\hat{x}(\tau)$ represents the trajectory in the symmetry-reduced state space of the slice. The two trajectories are equivalent up to a rotational translation $g(\tau)\hat{x}(\tau)$. (b): A relative periodic orbit passes through $x(0)$, $x(\tau)$, and $x(T_p)$, returning to the point $x(0)$ after a time translation T_p . Within the slice we see the symmetry-reduced periodic orbit in which $\hat{x}(0) = \hat{x}(T_p)$. Adapted from [CBEC⁺12].

a structure is very difficult to conceptualize, and nearly impossible to analyze. However, with an approach called the *method of slices* [CBEC⁺12], we can turn the relative periodic orbit into an ordinary periodic orbit that can be analyzed, and can provide us with useful statistics about the flow. In order to do this, we will take a “slice,” so to speak, of this torus, in order to obtain a representative profile of the most common periodic orbits that, outside of our slice, occupy very different locations in state space. We will then process the slice around the torus, observing only the changes in the behavior of the orbits that take place within the slice, and leaving those behaviors “imprinted” on the slice as it progresses, in a manner of speaking. Because we are concerned with behaviors that vary in location but not in structure, the method of slices reduces the system to a manageable state.

3 General Methods

Although the circularly-configured Kolmogorov flow has been little examined in an experimental scenario, its basic mechanics are comparable to those of the square setup, and in this thesis the methods of analysis will mark the primary difference between the two. In this chapter, we will discuss the basic experimental methods that were used in both the square and the circular configurations, before moving into separate discussions of each experiment.

3.1 Forcing

In order to create the desired flow profile, we obviously needed some way to make the fluid move. Although it could be possible to create Kolmogorov flow mechanically, there is another way that is almost certainly less expensive, less complicated, and less prone to undesired behavior. This method, which we used, relies on the Lorentz force

$$\vec{F} = \vec{J} \times \vec{B}, \quad (3.1)$$

in which \vec{J} represents the current density vector, or the amount of electric current per area, and \vec{B} the magnetic field vector. This relationship gives us a very convenient way to apply a force to a fluid— one must only supply a current and a magnetic field, and the fluid will follow the force. It is relatively easy to create specific flow profiles using this method, as the parameters involved therein can easily be changed to suit one's needs. In order to increase the magnitude of the force, one can simply increase the voltage applied to the working fluid. In order to reverse the direction of the flow, the direction of the electric current can simply be reversed. Furthermore, the behavior of the flow can be altered by changing the position, size, shape, or quantity of magnets used to supply the magnetic field. The first of these techniques was used extensively in our experiment, as will be discussed shortly.

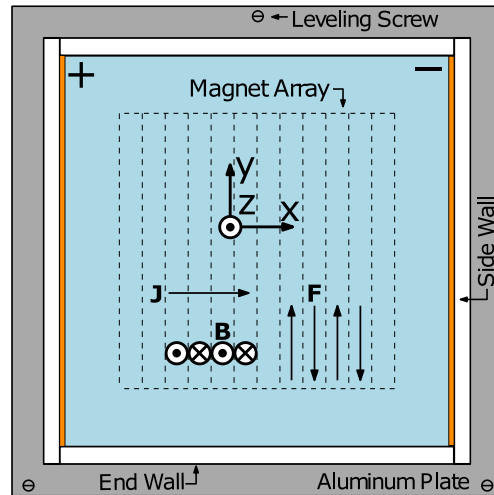


Figure 3.1: A schematic of the first experiment’s configuration, based on [TSKP⁺17].

3.2 Working Fluid

The fundamental elements of both configurations were based on tried-and true methods used to create quasi-two dimensional Kolmogorov flow in a laboratory environment [KO11]. For our working fluid, we chose copper sulfate pentahydrate ($\text{CuSO}_4 \cdot 5\text{H}_2\text{O}$), which has been the working fluid of choice in most similar experiments for several reasons. Firstly, because it is an electrolyte, $\text{CuSO}_4 \cdot 5\text{H}_2\text{O}$ is highly conductive, which essentially means that for a certain supplied voltage, it will achieve a greater current density than a less-conductive liquid like water. A second advantage of $\text{CuSO}_4 \cdot 5\text{H}_2\text{O}$ is that it is copper-based, which helps to mitigate any unwanted electrochemical interactions between it and the copper electrodes used in our experiment. Although the fluid did leave deposits on the electrodes in the flow tank, these deposits were essentially pure copper and therefore did not impair the electrodes’ function. The fluid was made in the lab from copper sulfate crystals dissolved in water. Precise quantities of the crystals shown in Fig. 3.2 were used in order to ensure that the concentration of copper sulfate in the fluid would be consistent across all of our experiments.

In both experiments, the working fluid was placed in a tank, and the tank was placed on top of an array of magnets, so that the magnetic field would permeate the fluid. Copper electrodes were placed on the boundaries of the flow tank so that a current could run through the fluid, interacting with the magnetic field as discussed in Section 3.1 to create the desired force. A schematic of the first experimental configuration is shown in Fig. 3.1.



Figure 3.2: Copper sulfate pentahydrate crystals

3.3 Image Capturing and Processing

In order for us to analyze the flows in our experiments, we had to record them. In order to do so, we used several different cameras, but our methods of recording were similar. In both cases, the camera was positioned directly above the flow tank and oriented so that it pointed straight down. Lighting was supplied by two small LED studio lights. These were positioned near the sides of the flow tank, rather than above it, in order to mitigate the amount of light that might otherwise have reflected off the surface of the fluid into the lens, creating glare.

Images were generally captured by recording videos of the desired flow behaviors. Videos, however, were of relatively little use to us inasmuch as they could not be processed by our particle image velocimetry (PIV) software, the powerful analytic tool we will discuss shortly. In order to process the information captured in the video files, we used Python code, including the OpenCV library, to break up each video file into a large number of image files. For instance, in our first experiment, our camera recorded video at a frame rate of 24 frames per second. As a result, when we recorded approximately forty seconds of video, it took the unfortunate lab computer quite a while to extract and save nearly a thousand separate image files, which then had to be analyzed.

3.4 JPIV

At this point we must discuss one of the most essential elements of our experiments: particle image velocimetry (PIV). For years, PIV has been nearly ubiquitous in experimental fluid dynamics, because it allows velocity vector fields to be created from digital images of a flow [AW11]. In basic terms, PIV software is fairly simple. First, the user provides a PIV program with two or more images (we

will just imagine that it is two for now). The PIV software then compares the two images, looking for differences between them. Any differences are quantified by vectors, each vector showing the direction and magnitude of a specific difference.

This is, however, a huge oversimplification of how PIV actually works. In reality, PIV software does not compare images in their entirety. It actually employs a lattice of overlapping rectangular areas, sometimes known as *interrogation boxes*, to precisely scan the images. This complex approach is necessary because the images processed by the PIV software may contain a great number of small differences, and it is necessary to break the images up in order to mitigate the risk of mistaking one difference for another. This and other aspects of PIV software are explained in greater detail in Appendix A.

Luckily for those in the field of experimental fluid dynamics, there are numerous different ways to acquire PIV software, many of them at no charge. Python is a common vehicle for open-source PIV software, and we initially considered several different Python PIV packages, but in the end we decided on a Java-based freeware program called Java Particle Image Velocimetry (JPIV). Although we were quite a bit less familiar with the Java language than with Python, JPIV had a number of very appealing qualities. First, like a lot of other PIV software, it could be downloaded for free. However, unlike most other PIV software, it came with its own Graphic User Interface (GUI), which made it simple and intuitive to use. Instead of typing in commands, we were simply able to click on clearly-labeled buttons, and the various parameters of the PIV analysis could be altered with ease. Another particularly useful function was the ability to process large numbers of image files at once. That is, JPIV allows the user to upload a large number of image files, and then specify how the images are to be paired up and processed. For instance, after uploading a group of images, JPIV can analyze them sequentially (1 and 2, 2 and 3, 3 and 4, etc.), or in sequential pairs (1 and 2, 3 and 4, etc.). When each analysis is complete, JPIV creates a new file containing the information for the vector field. An advantage of these files is that each one is essentially a text file containing a huge array of numbers, which takes up much less data storage space than a conventional image file. JPIV has its own system for visualizing the vector field files, which includes a number of useful tools. The color-coding tool proved to be one of the most useful of all for understanding flow behavior, and an example of its use is shown in Fig. 1.2.

4 Square Configuration

In this chapter we will discuss the aspects of our first experiment which were unique to it. We will begin with our image capturing techniques and the particulars of the camera used in the experiment. Next, we will examine the flow tracers used to visualize the movement of the fluid. We will also discuss the PIV software used to analyze the flow images, and finally we will review the results, successes, and shortcomings of this experiment.

4.1 Methods

The “square” experiment was based mostly on tried-and-true methods for generating Kolmogorov flow. As discussed before, the Lorentz force was used to create the flow profile, and the voltage between the electrodes was increased or decreased as necessary in order to increase or decrease the magnitude of the force. By altering the force, we were able to alter the Reynolds number Re until a noticeable bifurcation occurred in the flow, the reasons for which are discussed in Chapter 2. Inasmuch as this particular flow profile had already been explored experimentally a number of times by others, the goal of this experiment was not so much to learn anything particularly new about the flow profile, but rather to familiarize ourselves with JPIV and to determine how we might best use it in our second experiment.

4.1.1 Image Capturing

In our first experiment, we used a GoPro[®] camera. These cameras have several advantages, as well as drawbacks, which merit discussion. First of all, as most people are probably aware, GoPro cameras are small, simple, and very user-friendly. Additionally, newer units can be connected to an app on one’s smartphone, which enables the user to see what the camera “sees” on the smartphone and control most of the camera’s settings and functions remotely. The ability to remotely

trigger the camera’s shutter release and video-recording functions was particularly useful for us, because manually pushing the record button had a tendency to shake the camera and disturb its precise positioning.

The GoPro, however, was not exactly made for use in a laboratory, and this reality made itself known to us in several ways. Firstly, the default settings on the GoPro made full use of its slightly fish-eyed lens, which was decidedly not optimal for our purposes. The distortion typical of a fisheye lens would have very noticeably thrown off the PIV analysis, if we had not found a way to restore the image style to a linear format. Secondly, we found that the GoPro’s overall simplicity was occasionally a bit of a detriment, because its settings could not always be customized to suit our needs. This being said, however, we were able to use the GoPro more or less effectively throughout the first experiment.

Because the goal of our first experiment was essentially to perfect our methods of analysis in preparation for the second experiment, we tried several methods of recording. One method involved using the “burst” mode on our camera to take 30 pictures over a span of one second. This method had several advantages; first and foremost, in burst mode the camera captures images, rather than a video, which was convenient because JPIV software can only analyze image files. Secondly, the image files captured in burst mode are relatively high-resolution compared to the images that can be extracted from a video file, as we will discuss shortly. This high resolution allowed for more detailed analysis by JPIV, and thus a more informative vector field. There was, however, a major drawback of burst mode which ultimately rendered it untenable—namely, burst mode can only record for one or two seconds at a time. While we were often able to extract visually appealing data from the images captured with burst mode, we found that experimentally significant flow behaviors tend to take place over the course of at least five or ten seconds.

For the remainder of our first experiment, we recorded primarily videos of the flow, in order to capture bifurcations taking place over a longer period of time. This proved to be relatively simple, although there were one or two drawbacks to video recording. As mentioned in the previous chapter, because JPIV could not analyze video files, we had to use Python to break each video file into its constituent frames. In computer terms, this was bound to be a simple but rather time-consuming process, because image files tend to take up a fair amount of space. Python, however, was able to accomplish it with no supervision necessary, making it practically an afterthought, rather than a chore.

4.1.2 Flow Tracers

In order for PIV software to function properly, it must be able to perceive differences in the positions of distinct objects between adjacent images. If we had

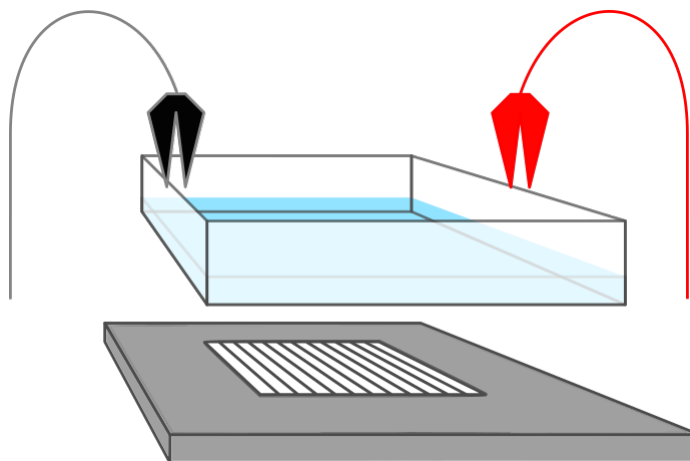


Figure 4.1: The essential elements of the “square” experimental setup, from top to bottom: the positive and negative electrical leads, the transparent acrylic flow tank, and the aluminum base plate with inlaid neodymium magnets. Not shown are the three threaded micrometer heads that were used to level the base plate.

only taken photos or videos of the copper sulfate fluid by itself, there would have been very little for the software to pick up on, because the fluid is transparent and fairly uniform in appearance. In order to make the flow’s behavior readily apparent, we relied on yet another longstanding method: floating flow tracers. In our case, we used tiny hollow glass spheres, generally about $60\ \mu\text{m}$ in diameter. These flow tracers are so small and light that they take the form of a fine white powder. Although this might seem like an odd way to visualize flow behavior, glass microspheres are in many ways optimal for this purpose. Because they are hollow and made of glass, they are highly reflective, and in fact larger glass microspheres are incorporated into many types of highly reflective paint used on roads and signs. Their light weight and buoyancy enable the microspheres to float on the surface of the fluid, which is highly important. In this experiment, we aimed to approximate the flow as quasi-two dimensional, so we were only interested in analyzing the flow on the very surface of the fluid layer, which was actually about five millimeters deep. The flow tracers can be seen in Fig. 4.2.

4.2 Analysis

As previously mentioned, JPIV was central to our analysis. In order to create the necessary vector fields, the image files taken from our videos were fed into JPIV, which then began the relatively slow process of creating vector fields from image pairs. JPIV’s built-in batch filtering scripts were then used to eliminate any bad vectors (discussed further in Sections 4.3 and 4.4), and the parameters of the

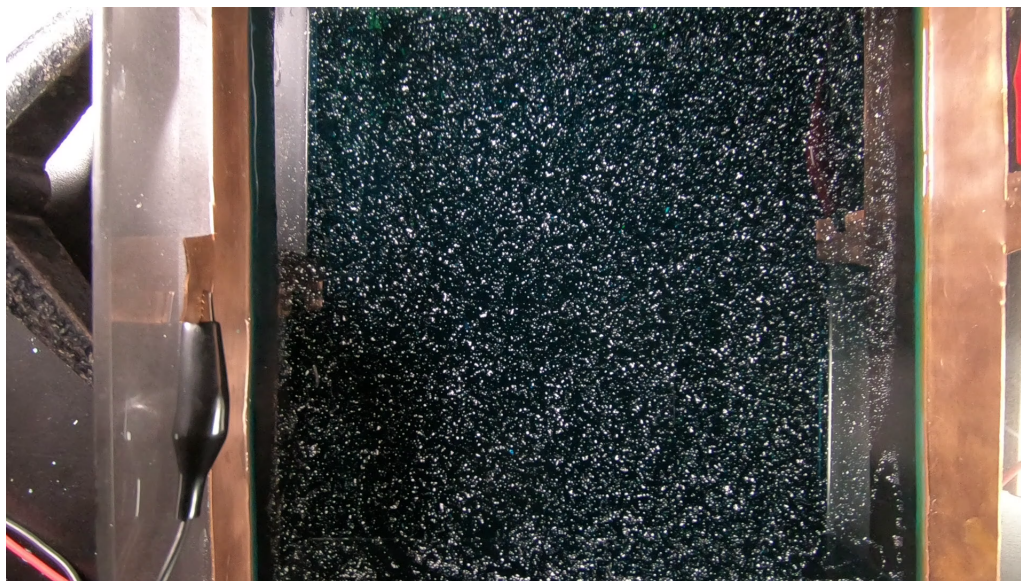


Figure 4.2: A frame from a video taken in the lab, showing the glass flow tracers suspended on the surface of the fluid. Each small white dot is actually a group of glass microspheres, which are drawn towards each other by effects related to the surface tension of the copper sulfate pentahydrate fluid. The copper electrodes in the flow tank are also visible on the left and right sides of the flow tank.

vector field viewing window were adjusted to optimize how the information was displayed. Although the vector fields were often informative and quite visually appealing right off the bat, JPIV's post-processing tools were really what allowed us to extract meaningful information. Perhaps the most important of these was the *normal vorticity script*. Vorticity is perhaps one of the most conceptually simple phenomena found in fluid mechanics—it essentially describes the spinning motion around a point relative to the flow of the fluid at that point. After this script was used to analyze the vorticity of the vector fields, JPIV's color-coding parameters could be set to show the vorticity on a red-blue spectrum in which blue coloration represents negative, or clockwise vorticity, and red coloration represents positive, or counterclockwise vorticity. Although the color coding could be used to show various other aspects of the vector field, such as vector magnitude in the horizontal or vertical direction, vorticity was of primary interest to us because in Kolmogorov flow vortices are the primary indicator of flow behavior.

Although these vector fields were more or less the final result of our analysis, and JPIV offered numerous tools for analyzing them, we wished to take our analysis one step further by making a video from the vector fields, so that we could watch how they changed in real time as the flow bifurcated. Luckily, JPIV is equipped with a script file that enables large numbers of its vector field files (with the .jvc file extension) to be converted into JPEG, PNG, TIFF, or other

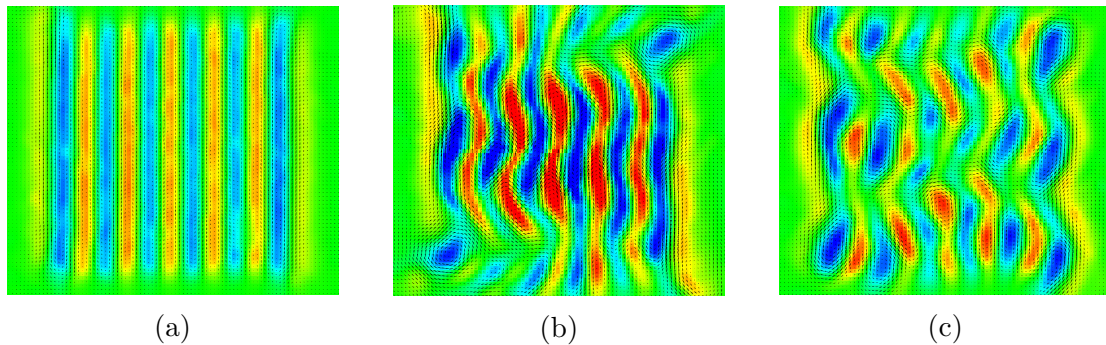


Figure 4.3: A sequence of three frames taken from the initial stage of a forty-second analysis of a flow bifurcation, in which the voltage between the electrodes was slowly raised from 0 to 12 V DC. (a), (b), and (c) show, in order, the first, 200th, and 400th frames out of a total of 869. The flow is initially laminar, but by the 200th frame the stripes have begun to distort, and by frame 400 the flow is beginning to resemble a lattice of vortices, rather than an array of adjacent stripes.

image files. So essentially, we repeated our previous image-processing, only in reverse. We converted the vector field files into image files, then used FFmpeg, a command-line program available online, to “stitch” the image files together into a .MP4 video file.

4.3 Discussion

As our initial experimentation with the Kolmogorov flow was aimed at perfecting our methods of experimentation and analysis, it was inevitable that we would discover flaws and shortcomings in both, and discover these we did. Firstly, our flow tank had an open top, which led to issues with the copper sulfate fluid. When it was exposed to air for long periods, the water would slowly evaporate, leaving behind chunks of copper sulfate crystals and decreasing the thickness of the fluid layer. At first, this effect seemed to have little impact on our experiment, but after several weeks we began to find that the flow was behaving abnormally. As a result, we resolved to develop an airtight (yet still transparent) lid for our flow tank, which we hoped would effectively resolve the problem.

Another issue in our experiment arose from the behavior of the flow tracers. We found that initially, the flow tracers would be evenly spread out over the surface of the fluid, as was necessary for JPIV to be able to create an accurate vector field. After periods of more than a few minutes, however, the flow tracers would form patches on the surface. These patches impeded the PIV analysis, because the areas between the patches were often devoid of flow tracers. Additionally,

the patches became large enough that they began to resist and impede the flow, causing unusual behaviors. In one of our last trials of the square configuration, we tried applying a very small amount of dish soap to the surface of the fluid, which greatly decreased its surface tension and caused the flow tracers to spread out, mitigating the clumping problem. However, the decreased fluid tension created a new problem: flow tracers began to sink due to the decreased surface tension, and after a while the surface of the fluid layer had relatively few flow tracers on it. It is entirely possible that a smaller amount of dish soap would have had the desired anti-clumping effect, without causing the sinking problem.

Lighting proved to be another difficulty in our setup. The flow tank was lit by two miniature LED studio lights, and while these provided more than enough light for the entire flow tank, they had to be positioned very carefully in order to mitigate the amount of light that would reflect off the surface of the fluid layer and hit the lens, causing glare. This proved to be a particularly tricky problem to solve, because most of the possible solutions, such as positioning the lights further from the tank, would impair the effectiveness of the lighting, thus making the PIV analysis less accurate, thereby causing the same problem that the solution was meant to solve. Altogether, this was not a problem that we were able to definitively solve, although we were able to position the lights such that the resulting glare in the resulting images was confined to the periphery of the flow tank. This glare can be seen in Fig. 4.2, near the upper left and lower right corners of the flow tank.

Finally, we found that in our PIV analysis, there would often be strange patterns of bad vectors, usually arranged in a thin horizontal line across all or part of the screen. Although these bands could be removed using JPIV's filtering scripts, this was more of a cure than a prevention, as we were only able to smooth over the bad data, and unable to recover the proper data. Numerous attempts to prevent this problem from occurring proved somewhat effective, although we could not conclusively determine whether our attempts to eliminate the distortion were successful, or whether the distortion was disappearing and reappearing completely by coincidence. Fig. 4.4 shows an example of the linear distortion.

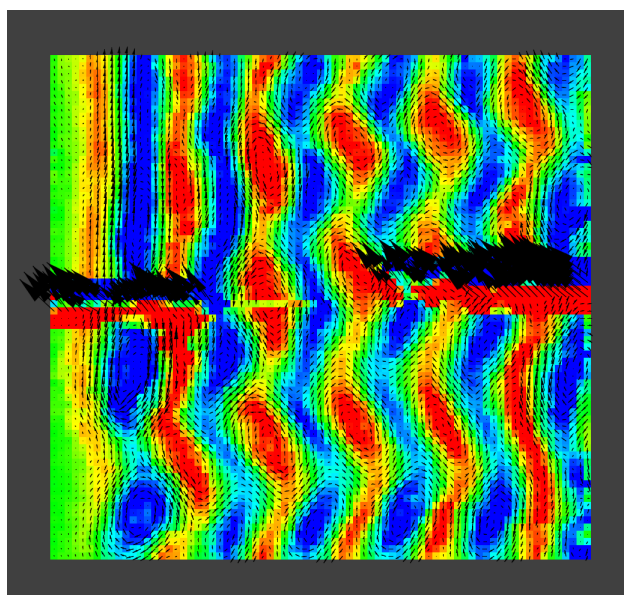


Figure 4.4: This frame from one of our flow videos shows the linear distortion which plagued our analysis.

5 Circle Configuration

Our second experiment resembled the first in many ways; the working fluid, the implementation of the Lorentz force, and the overall method were essentially identical. The primary difference was that in place of our previous square flow tank, we used a circular flow tank. To be more precise, we used a ring-shaped flow tank which had been 3D-printed by a previous student in the same lab, namely, Ruvim Kondratyev of the class of 2017. Kondratyev's thesis revolved around a quasi-two dimensional fluid simulation of black hole accretion disk behavior, and so it had incorporated essentially all of the elements we needed for our work. In fact, in our first experiment, the copper sulfate fluid we used was left over from Kondratyev's work. So, with great appreciation for both time and money saved, we incorporated much of his equipment into our second experiment.

5.1 Methods

The idea of a circular flow configuration is conceptually simple, but experimentally it posed a couple of challenges. First and foremost was the question of how the magnets were to be configured. In the previous experiment, we had been able to use long bar magnets, which were obtained with relative ease and which were easy to position in the aluminum base plate. It is unlikely that we could have acquired flat ring-shaped Neodymium magnets, as Neodymium is very brittle and it would be rather difficult to produce such a magnet, to say nothing of the relative lack of consumer demand for such a niche product. Here we took advantage of Kondratyev's greatest creation: a cylindrical base with a great number of magnet-holding holes arranged in concentric rings, shown in Fig. 5.1. The only inconvenience posed by this device was the orientation of the magnets. Kondratyev's thesis had required a simulation of a fluid disk moving entirely in one direction of rotation, but our experiment necessitated counter-rotating flow bands. To accomplish this, we had only to remove half of the magnets from their holes, flip them upside-down, and place them back in their holes. Kondratyev, in his

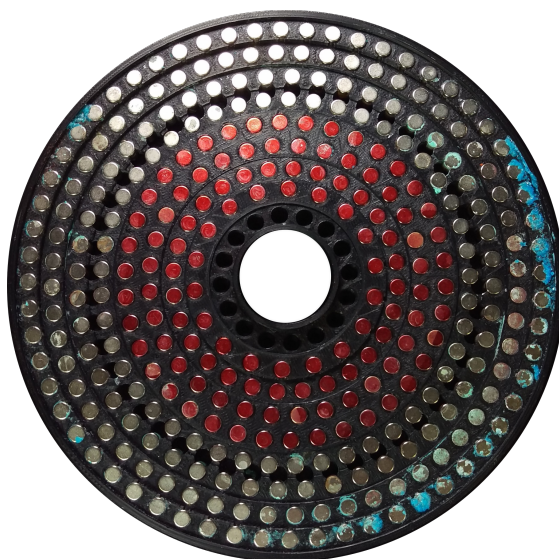


Figure 5.1: Ruvim Kondratyev’s 3D-printed baseplate, with its concentric rings of Neodymium magnets. The red color of the inner rings was added to signify that they were positioned upside-down relative to the magnets in the outer rings. Copper sulfate crystals have noticeably formed at the right and bottom of the plate as a result of a minor fluid leak.

wisdom, had designed the magnet holder so that under each magnet a small hole protruded through the bottom of the holder. These holes, just large enough to permit the end of a paper clip, allowed us to push the magnets out of the holder. Flipping the magnets, however, proved to be more difficult than we had expected, as the magnets were much more inclined to stick to their neighbors than to be stuck back in their holes. In the end, all of the magnets in the inner four rings (out of a total of eight rings) were repositioned to create the desired two flow bands.

In addition to the magnet holder, the second experiment’s flow tank was also a holdover from Kondratyev’s work, and had been 3D-printed specifically to work in tandem with the magnet holder. Similarly to the previous experiment, strips of copper were used for the electrodes. They were wrapped around the outside of the inner wall and the inside of the outer wall, and connected to the power source with alligator clips. Because the magnet holder had no leveling apparatus, it was placed on top of the aluminum plate used in the first experiment, and the flow tank was placed on top of it.

In this experiment, rather than using the hollow glass microspheres we had used previously, we wanted to try our hand(s) at making fluorescent flow tracers, with the idea that these would be more visible, and that they would allow us to use more light-filtering techniques in our analysis. In order to produce fluorescent flow tracers, we mixed Rhodamine 6G, a powdered xanthene dye, with a liquid

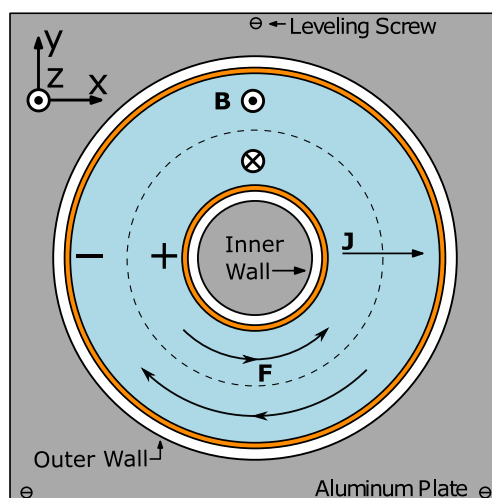


Figure 5.2: The circular flow configuration had only two flow bands, as opposed to the square configuration's twelve.

polyester casting resin. A catalyst was added, and after the mixture had hardened, it was broken up with a hammer. The small pieces were then ground up in a coffee grinder, and put through a series of sieves. The sieves separated the particles in increments of 106, 90, 53, and 45 μm . After being sieved, the particles were separated by size, so that if any problems were caused by the size of the particles, a different size could be used. The largest particles were generally avoided, as they had a tendency to sink in the fluid. The smallest particles also were not often used, because they were difficult to distribute across the surface of the fluid and they did not reflect light as well as the larger sized particles.

Rhodamine fluoresces orange when exposed to green light, so in order to take advantage of this effect we attached an array of green LEDs to the cardboard lens collar we had used in the previous experiment and positioned it above the flow tank. We then placed a green-light filter over the lens of the camera. By doing this, we could ensure that the flow tracers would be as visible as possible by minimizing their green-illuminated surroundings.

A new camera was used in this experiment. Although the GoPro had served our needs relatively effectively, it had a number of shortcomings which were more or less resolved by the IDS uEye[®] camera. The GoPro is intended to be very user-friendly and intuitive, which unfortunately means that many of its image-collecting parameters such as its focus and aperture cannot generally be controlled, as they are automatically set by the camera. uEye cameras, on the other hand, are generally designed for industrial or commercial imaging and can be configured in a variety of ways to suit one's needs. Whereas the GoPro was operated either from its own interface or by means of a mobile phone app, which often disconnected from the camera abruptly, the uEye was a USB camera, meaning that it was connected

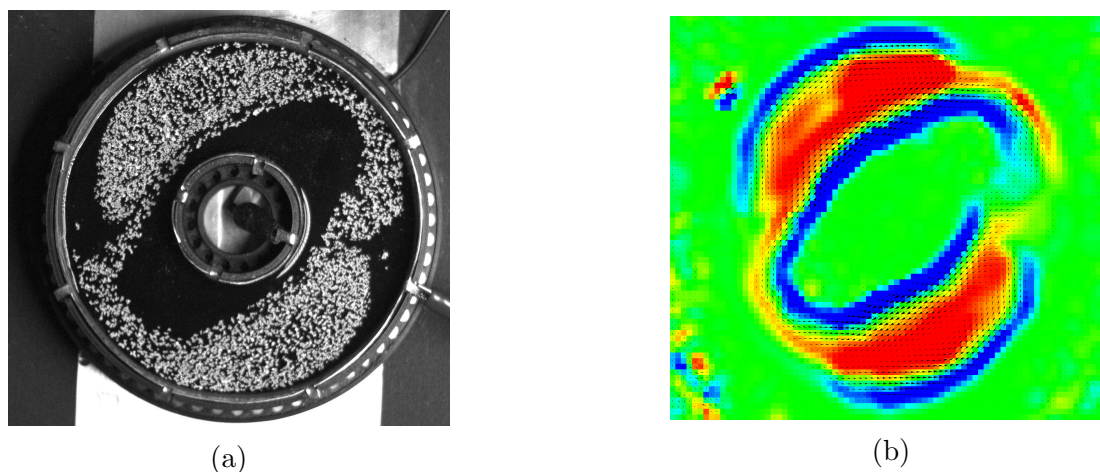


Figure 5.3: Two different views of the circular Kolmogorov flow after its primary bifurcation. (a) shows the camera’s view—note that although the camera used in the second experiment shot in monochrome, the fluorescence of the rhodamine-resin flow tracers can still be observed. (b) shows the image resulting from PIV analysis, color coded for vorticity. The areas of strong clockwise (blue) vorticity represent boundary effects created by the walls of the tank and by the “football”, rather than areas of actual strong clockwise vorticity.

to a computer by a cable, and was operated by a program on the computer. This program allowed for extensive modification of the camera’s parameters, which was quite helpful in our experiment.

Despite the difference in cameras, our experimental method was largely the same. Each experimental trial essentially involved starting the flow at a low current value, ensuring basic laminar flow, then slowly increasing the current until bifurcations occurred. These bifurcations were captured on our camera and the images were processed with JPIV.

5.2 Analysis

The method of analysis used in the circular configuration was essentially identical to that of the previous configuration. Using the software associated with the uEye camera, we recorded numerous videos with a specified number of frames in each video. These vector fields were color-coded based on their vorticity, an example of which is shown in Fig. 5.3b.

5.3 Discussion

In the end, time was insufficient to allow for a substantive analysis to take place. Although the fluorescent flow tracers were an effective and efficient means of visualizing the flow, the process of producing them proved to be rather inefficient. It took a great deal of time to grind up the plastic and sieve it into separate containers, and this process ultimately absorbed much of the time which, in retrospect, ought to have been spent preparing to conduct the analysis based on the method of sections and slices discussed earlier. However, the behavior observed in the fluid merits discussion. Inasmuch as circular Kolmogorov flow has not been experimentally analyzed to an extensive degree, we were not entirely sure what behaviors would occur when the flow bifurcated. The behavior shown in Fig. 5.3 occurred after the primary bifurcation, but it is of course unclear what the primary bifurcation behavior would look like in a system with more flow bands. In any case, the primary bifurcation behavior of the system was surprisingly resilient to changes in the current. As the current was raised, the two main vortices remained relatively unchanged despite the rapid flow of the fluid. This could perhaps be a subject of further analysis in future work on this topic, aside from the primary analysis concerned with sections and slices.

5.4 Conclusions

It is no secret that time, or rather the lack thereof, is often a pernicious enemy of research. The relative material and procedural simplicity of our experiments meant that progress was fairly constant, and we faced few major setbacks. However, despite all this, the process of data collection proved to be a slow one, and a great deal of time was spent in determining the proper arrangements of various elements of the experiment. Furthermore, we found ourselves faced with numerous small problems that, although not particularly severe, nevertheless required a substantial investment of time in order to solve, an investment that occasionally came to nothing.

The copper sulfate fluid posed a problem inasmuch as, if left exposed to air, the water would evaporate out of the fluid, leaving only the $\text{CuSO}_4 \cdot 5\text{H}_2\text{O}$ behind in the form of a hard, crystalline crust (see Fig. 5.1). Although the evaporation was a slow process, it was nevertheless a problem inasmuch as the fluid was often left sitting in the flow tank for weeks on end. Although it never sat long enough for the fluid to evaporate entirely, even a small amount of evaporation was problematic because any change in the depth of the fluid layer could potentially alter the behavior of the flow. Furthermore, the evaporation left behind small, solid crystals at the bottom of the tank that tumbled around during experiments and may have interfered with our PIV analysis. We attempted to improvise several different

solutions to this problem using materials readily available in the lab, but none of our ideas proved to be particularly effective. Our initial attempts revolved around the concept of a glass cover on top of the flow tank, which would allow imaging while preventing air from escaping. Although the glass covers did not affect the quality of the images taken by the camera, they proved ineffective at preventing the fluid from evaporating. Future experiments would certainly be expedited if a better means of sealing off the flow tank from outside air (while still allowing the camera to see the fluid) could be achieved. In reality, though, it is not exactly necessary for the fluid to be covered at all times. As long as images are taken over a relatively short period of time (a few hours at most), it is unlikely that a significant amount of evaporation would result from the flow tank being uncovered. Therefore, if a potential cover could completely seal off the flow tank while being so opaque, rough, or reflective as to necessitate removal before imaging, it could still be highly beneficial. That being said, if a cover could completely seal off the tank while still allowing imaging, it would provide the additional benefit of preventing unwanted air currents and temperature changes from affecting the flow.

The 3D-Printed elements of the circular experiment, despite their innovative design, proved to be somewhat flawed. The magnet-holding base and the flow tank, despite being designed to fit together, were not quite happy with each other, and it was often rather difficult to position the flow tank precisely over the center of the magnet base. This possible minor misalignment of the magnets may have thrown off the behavior of the flow to some degree. Secondly, in our experiments it was very important to maintain a level surface for the fluid. Although the aluminum base plate did its part beautifully, the flow tank which sat above it left something to be desired. An examination with a bullseye level showed that the center of the tank was distinctly higher than the outer edge. It is possible that the tank was removed from the 3D printer when its plastic was still soft, thus causing a deformation. While a discontinuity in the level of the bottom of the tank would of course not affect the levelness of the fluid's surface layer, it would invariably affect the depth of the fluid, which we wished to be constant. Ultimately, it is hard to tell whether this had an effect on the behavior of the fluid, but we can certainly assume that a more uniformly level surface would have served us better.

Unfortunately, this thesis cannot be said to have achieved anything particularly spectacular. If nothing else, though, we have still shown one valuable thing—that even with relatively cheap and simple materials, it is possible to create a Kolmogorov flow profile which matches the predictions of other published trials. It bears noting, furthermore, that the exploration of the circular Kolmogorov flow by no means ends here. If, in the end, the work involved in the writing of this thesis goes towards laying the groundwork for future analysis, then something has still been accomplished here.

Bibliography

- [AW11] Ronald J. Adrian and Jerry Westerweel, *Particle image velocimetry*, Cambridge University Press, Cambridge, 2011.
- [BBM⁺99] John M. Burgess, C. Bizon, W. D. McCormick, J. B. Swift, and Harry L. Swinney, *Instability of the Kolmogorov flow in a soap film*, *Physical Review E* **60** (1999), 715–721.
- [Bey13] Wolfgang Beyer, *Mandelbrot set*, <https://wolfgangbeyer.de/chaos/chaos.htm>, October 2013.
- [CBEC⁺12] Predrag Cvitanović, Daniel Borrero-Echeverry, Keith M. Carroll, Bryce Robbins, and Evangelos Siminos, *Cartography of high-dimensional flows: a visual guide to sections and slices*, *Chaos* **22** (2012), no. 4, 1–10.
- [Cvi13] Predrag Cvitanović, *Recurrent flows: the clockwork behind turbulence*, *Journal of Fluid Mechanics* **726** (2013), 1–4.
- [KO11] Douglas H. Kelley and Nicholas T. Ouellette, *Using particle tracking to measure flow instabilities in an undergraduate laboratory experiment*, *American Journal of Physics* **79** (2011), no. 3, 267–273.
- [KUvV12] Genta Kawahara, Markus Uhlmann, and Lennaert van Veen, *The significance of simple invariant solutions in turbulent flows*, *Annual Review of Fluid Mechanics* **44** (2012), no. 1, 203–225.
- [LK15] Dan Lucas and Rich R. Kerswell, *Recurrent flow analysis in spatiotemporally chaotic 2-dimensional Kolmogorov flow*, *Physics of Fluids* **27** (2015), no. 4, 1–27.
- [Set09] Dr. Gary Settles, *Laminar-turbulent transition*, <http://www.flovizinc.com/index.html>, March 2009.

- [STGS18] Balachandra Suri, Jeffrey Tithof, Roman O. Grigoriev, and Michael F. Schatz, *Unstable equilibria and invariant manifolds in quasi-two-dimensional Kolmogorov-like flow*, Phys. Rev. E **98** (2018), 023105.
- [STM⁺14] Balachandra Suri, Jeffrey Tithof, Radford Mitchell, Roman O. Grigoriev, and Michael F. Schatz, *Velocity profile in a two-layer Kolmogorov-like flow*, Physics of Fluids **26** (2014), no. 5, 053601.
- [Str94] Steven H. Strogatz, *Nonlinear dynamics and chaos*, Perseus Books, Reading, MA, 1994.
- [The92] André Thess, *Instabilities in two-dimensional spatially periodic flows. part I: Kolmogorov flow*, Physics of Fluids A: Fluid Dynamics **4** (1992), 1385–1407.
- [TSKP⁺17] Jeffrey Tithof, Balachandra Suri, Ravi Kumar Pallantla, Roman Grigoriev, and Michael F. Schatz, *Bifurcations in a quasi-two-dimensional Kolmogorov-like flow*, Journal of Fluid Mechanics **828** (2017), 837–866.

A Code Used in Image Processing

A.1 FFmpeg

This code was used to combine image files into a video file. It was used in the standard Windows command console.

```
cd "imagepath"  
  
C:\ffmpeg\bin\ffmpeg.exe  
-r FPS -start_number K  
-i "imagepath\filename_%Nd.png"  
-c:v libx264  
-vf "fps=25,format=yuv420p"  
C:\outputfilename.mp4
```

The following arguments must be specified:

- On the first line, ““imagepath”” is the path of the folder containing the images which are to be stitched together. For example, if my images are contained in my “documents” folder, my path will be:

```
"C:\Users\louis\Documents"
```

Note that to make this step easier, one can copy the address of a folder in Windows by holding the shift key and right-clicking on the folder, then clicking “copy as path”. Also note that in this line, the single set of quotation marks must be included around the path.

- The second line specifies where FFmpeg is installed. If it is installed in a different location, this line will need to be changed to reflect its installation path.

- On the third line, “FPS” specifies the desired framerate of the video to be created. Remember that this code was used in our experiment to create videos from images of vector fields which had been created from images taken from videos of the flow. Therefore, in order for the vector field video to correctly represent the behavior of the flow, its framerate ought to match that of the original flow video.
- Also on the third line, “K” is the number attached to the first image file. Note that this assumes the image files are numbered sequentially (for example, file001,file002,file003, etc.). If the image files are created by JPIV, as ours were, they will be numbered in such a way.
- On the fourth line, “filename_” specifies the names of the image files to be used. Note that the underscore should only be included if there is an actual underscore in the filenames.
- Also on the fourth line, “N” specifies the number of digits in the numbers of the filenames. For example, if the file numbers start at 000 and end at 999, “N” will be three.
- On the seventh line, “outputfilename” is the desired name of the video file which will be created.

A.2 OpenCV

```

    # -*- coding: utf-8 -*-
    """
    Created on Thu Oct 25 09:43:28 2018

    @author: louis
    """

import cv2
import time
import os

def video_to_frames(input_loc, output_loc):
    """Function to extract frames from input video file
    and save them as separate frames in an output directory.
    Args:
        input_loc: Input video file.
        output_loc: Output directory to save the frames.

```

```

Returns:
    None
"""
try:
    os.mkdir(output_loc)
except OSError:
    pass
# Log the time
time_start = time.time()
# Start capturing the feed
cap = cv2.VideoCapture(input_loc)
# Find the number of frames
video_length = int(cap.get(cv2.CAP_PROP_FRAME_COUNT)) - 1
print ("Number of frames: ", video_length)
count = 10
print ("Converting video..\n")
# Start converting the video
while cap.isOpened():
    # Extract the frame
    ret, frame = cap.read()
    # Write the results back to output location.
    cv2.imwrite(output_loc +
        "%#05d.jpg" % (count+1), frame)
    count = count + 1
    # If there are no more frames left
    if (count > (video_length-1)):
        # Log the time again
        time_end = time.time()
        # Release the feed
        cap.release()
        # Print stats
        print ("Done extracting frames.
            \n%d frames extracted" % count)
        print ("Elapsed time: %d seconds."
            % (time_end-time_start))
        break

input_loc =
"input filepath"
output_loc =
"output folderpath"
video_to_frames(input_loc, output_loc)

```

The following arguments must be specified

- “input filepath” is the path of the video file to be split up into separate image files. The path can be obtained by the method described in the FFmpeg code section.
- “output folderpath” is the path of the folder where the created image files will be placed.